Relaxation of Optically Excited *p*-Nitroaniline: Semiempirical Quantum-Chemical Calculations Compared to Femtosecond Experimental Results

Vadim M. Farztdinov, Roland Schanz, Sergey A. Kovalenko, and Nikolaus P. Ernsting*

Institut für Chemie, Humboldt Universität zu Berlin, Bunsenstrasse 1, D-10117 Berlin, Germany

Received: May 11, 2000; In Final Form: September 12, 2000

p-Nitroaniline (pNA) was examined with the semiempirical SAM1 Hamiltonian in vacuo and in water. Geometry optimizations were performed in the ground and the lowest excited state along the $-NH_2$ wagging and the $-NO_2$ twisting coordinate. The latter is shown to play a key role in the spectroscopy and dynamics of pNA. The strong charge-transfer (CT) absorption band is conformationally broadened. Red-edge excitation prepares the CT state with a distribution of $-NO_2$ conformations which is concentrated around the coplanar conformation with the benzene moiety. In water, C-amino and C-nitro stretching vibrations are also excited. The structural reorganization along those modes is assumed to occur on the same time scale as ultrafast polar solvation. In this case the relaxation dynamics in water after ∼100 fs consists mainly in an evolution of the $-NO_2$ twist distribution toward a deep minimum at the perpendicular conformation; the dipole moment change during that process has an upper limit of 2 D. Stimulated emission is observable for the first few hundred femtoseconds. Thereafter a multidimensional conical intersection with the ground state is reached. The S_1 population decay can be monitored independent from the twisting process by observing excited-state absorption at 4 eV. All of these predictions are consistent with recent pump/supercontinuum probe measurements of pNA in water.

Introduction

p-Nitroaniline has an intense absorption band in the near-ultraviolet to visible spectral region which depends strongly on solvent polarity (Figure 1) and thus indicates a large increase of dipole moment upon optical excitation. The electronically excited state is characterized by intramolecular charge transfer from the $-NH_2$ to the $-NO_2$ group. *p*-Nitroaniline represents one of the simplest compounds with intramolecular charge transfer and therefore served as an important model for theoretical[1−9] and experimental[10−25] studies of linear and nonlinear optical properties. A characteristic feature of pNA is the absence of any measurable fluorescence; instead, nonradiative deactivation proceeds very fast by intersystem crossing (ISC) and by internal conversion (IC) to the ground state. A recent subpicosecond study[24] did not detect stimulated emission with 300 fs time resolution. The ISC quantum yield was found to depend strongly on solvent polarity, changing from 0.4 in dioxane to 0.03 in water.[24] Whereas intersystem crossing was investigated in a number of publications,[21,24] the primary processes leading to internal conversion of pNA have not yet been studied in detail.

Recently we observed for the first time all stages of relaxation of pNA in water after excitation at 400 nm with 40 fs pulses[25] by measuring transient absorption spectra with the pump−supercontinuum probe technique.[26] The transient spectra were recorded in the range 300−700 nm and are reproduced in Figure 2. Negative induced optical density ΔOD around 400 nm is recognized as the bleached ground-state absorption spectrum and excited-state absorption (ESA) is responsible for the induced absorption band at 300 nm. But in addition to these two components we now observe negative ΔOD in a range from

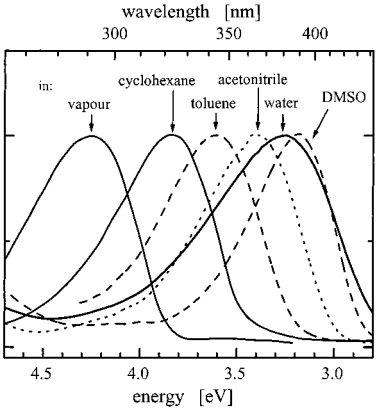

Figure 1. Absorption spectra of *p*-nitroaniline (pNA) in different environments, with band maxima scaled to a common value for better comparison.

430 to 700 nm where the sample was transparent prior to optical pumping. This signal therefore represents optical gain which is caused by stimulated emission (SE) transitions of excited pNA to the ground state. The SE band is seen to evolve to the red with an estimated dynamic Stokes shift of 4000 cm^{-1} during the first 100 fs. This is followed by a simultaneous decrease of the ESA and SE amplitudes over the next few hundred femtoseconds; thereafter a dispersion-shaped spectrum in the ground-state absorption region decays over picoseconds. These observations provide the motivation for the present quantum-chemical study of *p*-nitroaniline.

Let us review investigations pertinent to pNA. In a systematic study of substituted benzenes D-Ph-A, where D is an electron donor and A an electron acceptor, the spectral properties of absorption and emission were classified according to the donor and acceptor strengths (the "D/A index").[16] It was suggested

* Corresponding author. E-mail: nernst@chemie.hu-berlin.de.

10.1021/jp001690w CCC: $19.00
Published on Web 11/16/2000

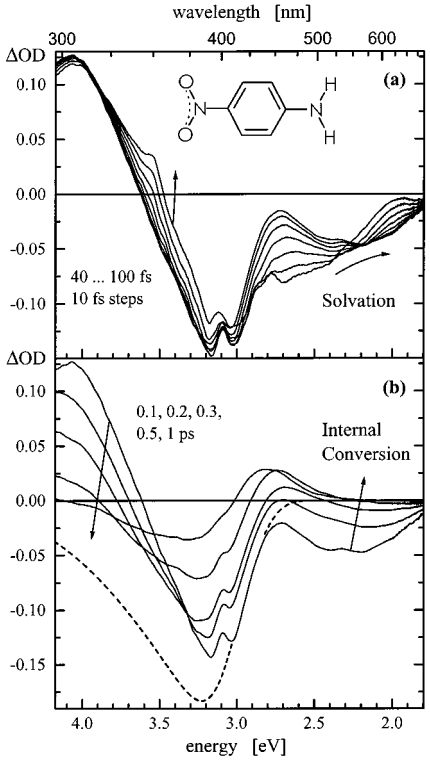

Figure 2. Transient absorption spectra of pNA in water after excitation at 400 nm with 40 fs pulses. The time delays of the spectra after excitation are given as insets. $\Delta OD < 0$ corresponds to ground-state bleaching (around 400 nm) or to stimulated emission (450−650 nm) while $\Delta OD > 0$ (around 310) indicates excited-state absorption. Arrows indicate the spectral evolution which is caused by solvation and $-NO_2$ twisting (a) and by internal conversion (b). For comparison, a scaled absorption spectrum is given as dashed line.

that the energy of the ^1L_a state gauges the degree of charge transfer and therefore can be used to parametrize the D/A index. For low D/A index, fluorescence is emitted from the lower ^1L_b state. For the amino donor and nitro acceptor the ^1L_b and ^1L_a states cross and fluorescence disappears. For larger D/A index the fluorescence reappears, this time from the ^1L_a state. One of the central questions is how the final polar excited state is reached, i.e., how the molecular structure and the solvent configuration change after excitation and what is the electronic nature of the excited state along that change. The concept of twisted intramolecular charge transfer (TICT)[27] states that the most extensive charge transfer is achieved with completely orthogonal D and A π orbitals. Because this form is preferentially stabilized by a highly polar solvent, electronic excitation of a coplanar donor−acceptor structure should be followed by its twisting to the more polar perpendicular conformation. This idea was most intensely investigated with 4-aminobenzonitrile (ABN) and dimethylaminobenzonitrile (DMABN) where a strong donor is combined with a weak acceptor. Both molecules show quite different behavior upon photoexcitation in polar solvents: while the first does not change its structure,[28] regarding the second it now seems generally accepted that the molecular reaction coordinate toward the final polar emitting state is $-NR_2$ twisting (see refs 29−32 and references therein). Nitrobenzene may be considered as having a strong acceptor without donor. A recent CAS-SCF study[33] showed that optically excited nitrobenzene relaxes along a $-NO_2$ wagging coordinate.

In excited *p*-nitroaniline, both the strong donor and the strong acceptor may alter their conformation, leading to increased intramolecular charge separation. Twisting of the nitro group relative to the central benzene moiety was addressed in ref 18. The dipole moment in the ground and excited state of planar and twisted nitroaniline and of derivatives was studied there experimentally by electrooptical absorption (in dioxane) and theoretically with empirical modifications of Hückel's molecular orbital theory. It was shown that in the excited state the dipole moment is larger when the $-NO_2$ is twisted compared to the coplanar conformation and that the twisted state is stabilized in highly polar solvents. Considerable deviation from the coplanar $-NO_2$ conformation was observed for 3,5-dimethyl-4-nitroaniline in the ground state because of the steric effect of the ortho methyl groups. The angle between the benzene moiety and the $-NO_2$ group for this compound was estimated[18] to be nearly 60°.

In this paper we examine the photoinduced processes of pNA in the gas phase and water and determine how these processes are recognized in the transient optical spectra of Figure 2. We find that a significant contribution to the width of the absorption band comes from conformational broadening. Just after the excitation in water, broad emission is expected which rapidly shifts to lower energy because of solvation coupled with vibrational redistribution, and further because of internal $-NO_2$ rotation. At a twisting angle of $\approx$60° the molecule enters an intersection region with the electronic ground state where internal conversion takes place effectively. The latter process may be monitored by excited-state absorption.

Computational Methods

There are many different semiempirical and ab initio methods for quantum chemical calculations of large molecules (see ref 34 for a survey and original citations). As was pointed out in ref 24, a careful evaluation of the many theoretical calculations of pNA shows little agreement concerning the energy levels and electronic structures of the excited states. Even ab initio calculations[7] with complete active space multiconfigurational SCF (CAS MCSCF) electronic wave functions predict charge-transfer excitation energies of pNA in different solvents which overestimate the experimental ones by up to 1 eV. At the same time the agreement of the ab initio ground-state geometry with experiment[10] is rather good. Although a nonplanar structure was found to be slightly lower in energy, due to high cost and difficulty of ab initio calculations in most of them a planar C_{2v} structure was adopted.

We tested the following semiempirical methods: AM1, PM3,[34] and SAM1 (Semi-Ab initio Model 1, the latest product of Dewar's group),[35] all with complete active space configuration interaction (CI) and without. The semiempirical methods are not as time consuming as ab initio calculations and therefore allow us to fully optimize the structure in the electronic ground and first excited states. Almost all calculations were performed with the program package Ampac 6.02, some of them with the latest version 6.55.[36] The effect of polar solvents was treated with the conductor-like screening model (COSMO).[37] The SAM1 Hamiltonian is known to produce better results for heats of formation than AM1 and PM3.[35] For comparison we also performed ground-state geometry optimization ab initio at the RHF/6-31G level using Gaussian98.[38]

In Tables 1−3 we compare quantities for the optimized ground-state structure as calculated with the different methods and relate them to experiments. A survey of ground-state dipole moments (Table 1) shows that SAM1 gives values close to the experiment[39] and identical with the best ab initio data.[7] It also gives better results for the ground-state absorption spectra as judged by comparison with experiment (see the next sections).

TABLE 1: Comparison of Calculated Molecular Quantities of pNA in Vacuo with Experiment[a]

	SAM1	AM1	PM3	ab initio	experiment
ΔH_0 (kcal/mol)	11.8[35]	19.5[35]	10.7[35]		14.1[35]
	11.82	21.55	10.69		
$\theta_{pyr}(-NH_2)$ (deg)	25 (CI = 22)	24 (CI = 22)	43 (CI = 24)	35 SCF[6]	
				44 MP2[6]	
$\mu_0^{(0)}$ (D)	6.99	7.30	6.62	6.87 MP2[6]	6.3[b]
	6.48 (CI = 16)	7.22 (CI = 16)	6.72 (CI = 16)	7.3 MP2[9]	6.2[19]
	6.36 (CI = 22)	7.17 (CI = 22)	6.75 (CI = 24)	6.36 MCSCF[7]	
$\mu_4^{(0)}$ (D)	14.1 (CI = 22)	11.8 (CI = 22)	11.3 (CI = 24)	13.76 MCSCF[7]	13.5[18]
					14−15[13]
					15.2[39]

[a] ΔH_0 is heat of formation of the electronic ground state, θ_{Pyr} the $-NH_2$ pyramidalization angle, $\mu_0^{(0)}$ and $\mu_4^{(0)}$ are the dipole moment for ground state and the Franck−Condon excited state $S_4^{(0)}$, respectively. [b] The average over all corresponding data cited in ref 39.

TABLE 2: Optimized Bond Lengths (Å) of Ground-State pNA in Vacuo and Comparison with Literature Data[a]

bond	SAM1 (CI = 22)	SAM1 (CI = 22) rescaled	CPHF (ref 3)	MP2 (ref 6)	AM1 (CI = 16)	PM3 (CI = 16)	expt (ref 10)
H1−N1	0.991	0.991	0.992	1.004	0.987	0.988	1.01
N1−C1	1.381	1.352	1.374	1.379	1.368	1.383	1.35
C1−C2	1.439	1.409	1.409	1.411	1.422	1.412	1.41
C2−C3	1.413	1.383	1.382	1.394	1.390	1.386	1.37
C3−C4	1.420	1.390	1.395	1.398	1.405	1.404	1.39
C4−N2	1.493	1.461	1.445	1.465	1.479	1.488	1.45
N2−O1	1.229	1.229	1.243	1.247	1.207	1.219	1.23
C2−H3	1.090	1.067	1.071	1.086	1.104	1.099	
C3−H4	1.089	1.066	1.068	1.082	1.101	1.097	

[a] For atom numbers and bond angles see Figure 3a.

TABLE 3: Vibrational Modes of Low Frequency (cm^{-1}) of Ground-State pNA in Vacuo (cf. Figure 3)

		SAM1		AM1		PM3			
mode	assignment[a]	CI = 0	CI = 22	CI = 0	CI = 22	CI = 0	CI = 24	ab initio	experiment
ν_1	$\gamma^{as}{}_{NO2}$	41	12	57	44	32	93	71	57,[10] 53[14]
ν_2	11	105	106	100	99	96	100	125	115−215[40], 117[b]
ν_3,	15	196	202	220	220	221	224	248	228[c]
ν_4	10b	294	297	280	287	260	287	320	299[14]
ν_5	$\gamma^{s}{}_{NH_2}$	249	363	335	332	847	773	571	811[14]
ν_6	$\gamma^{as}{}_{NH_2}$	370	374	350	744	290	344	353	427[14]
ν_7	6a	382	390	404	400	371	370	394	358[40]

[a] Normal modes are labeled according to Varsanyi's nomenclature[40] for benzene derivatives. [b] Data[41] for aminobenzonitrile.

According to our experience, AM1 and P3 produces transition energies and oscillator strengths which are too low.

On the other hand, the bond lengths of a carbon atom with other atoms, as obtained with the SAM1 Hamiltonian, are larger than those from AM1 and PM3 Hamiltonians or ab initio calculations (Table 2). After rescaling our calculated C−X bond lengths with a factor 0.979 = 1.39/1.420 (which sets C3−C4 to the experimental value), all these bond lengths almost coincide with the experimental ones.[10] (A factor 0.980 needs to be applied to the SAM1 structure of benzene calculated with CI = 14.) The resulting geometry is given in Table 2 and compared to the literature.

On the basis of this comparative study we chose SAM1 to examine the photochemical processes of pNA in different solvents and find their spectral manifestations. Geometry optimizations were performed for the ground and the lowest excited state of pNA in the gas phase and in acetonitrile and water. We calculated also the S_0 potential energy surface in the following coordinates: twist and wag of $-NH_2$, and twist and wag of $-NO_2$. The most extensive calculations were done for pNA in water. Results depend on the number of molecular orbitals included into CI (as controlled by the parameter CI[36]): while there are sharp fluctuations for CI < 12, smooth behavior is obtained for CI > 12. A default 400 × 400 size of the configuration interaction matrix was used in CI calculations; an increase to 1200 × 1200 lowers excited states by ∼0.1 eV on average.

Results and Discussion

pNA in the Gas Phase. *Ground-State Geometry, Vibrational Modes, and Potential Energy Surface.* The calculated geometry for the ground state is shown in Figure 3a and the low-frequency modes are sketched in Figure 3b. The dependence of vibrational frequencies on the Hamiltonian is given in Table 3. We will need the wag and twist angles of the H_2N- and $-NO_2$ groups. These angles are defined (with $-NO_2$ as example) as $\varphi_{wag}^{nitro} = (\pi\text{-}\theta_{O1-N2-C4-O2})/2$ and $\varphi_{twist}^{nitro} = \theta_{O1-N2-C4-C5} - \varphi_{wag}^{nitro}$.[42] The molecule is essentially planar; only $-NH_2$ is slightly wagged ($\varphi_{wag}^{amino} \approx \pm 15°$). The structure agrees well with results from X-ray diffraction[10] which show a vibration of amino nitrogen normal to the molecular plane and considerable torsional activity of the nitro group with an estimated frequency of 57 cm^{-1}. Our calculations always predict $-NO_2$ twisting for the lowest mode; its frequency when averaged over all methods is 50 cm^{-1}. The accuracy for torsional frequencies with SAM1 is ∼50 cm^{-1} and torsional frequencies are usually underestimated by semiempirical methods.[43] The $-NH_2$ wagging mode is calculated (with

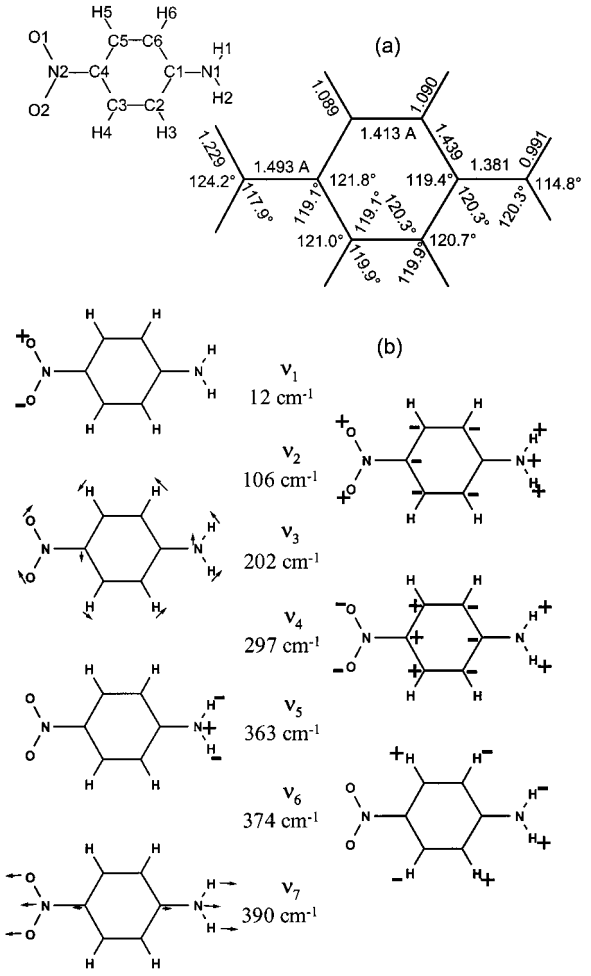

Figure 3. Geometry of ground-state pNA in vacuo (a) and schematic drawing of displacements for the low-frequency vibrational modes (b). Calculations for all figures were performed with the Semi-Ab Initio Model 1 (SAM1)[35] and configuration interaction is controlled by a parameter CI[36] (For this figure CI = 22.).

CI = 22) at 363 cm^{-1} close to the $-NH_2$ twisting mode at 374 cm^{-1}. The higher vibrational modes of a_1 symmetry, as calculated by us ab initio for the rescaled geometry, obtained with SAM1 (CI = 22) optimization, have frequencies which agree well with those in ref 8. [When ab initio RHF is used for optimizing the pNA geometry, we obtain the same vibrational frequencies except for the mode at 1467 cm^{-1} which we find at 1623 cm^{-1}.] Frequencies of modes involving mainly the $-NH_2$ moiety agree well with the corresponding (unscaled) frequencies of *p*-aminobenzonitrile[44] if calculated with the same PM3 method. Vibrational modes involving mainly displacements in $-NO_2$ change only little when $-NH_2$ is replaced by $-N(CH_3)_2$. For example, the $-NO_2$ twist mode remains at $\approx$50 cm^{-1}. But the frequencies of vibrations involving the amino moiety decrease: the $-N(CH_3)_2$ twist and wag modes are now located at 123 and 173 cm^{-1}, respectively. We will not discuss further the absolute values of vibrational frequencies (and therefore do not scale them) but shall later consider qualitatively how the low-frequency modes change with excitation and solvation.

To check whether the geometry in Figure 3a corresponds to a local or global minimum, the S_0 potential energy surface was scanned by varying coordinate pairs selected from the twist and wag angles of $-NH_2$ and the twist and wag angles of $-NO_2$. The results, some of which are shown in Figure 4, confirm that the geometry in Figure 3a corresponds to the global minimum.

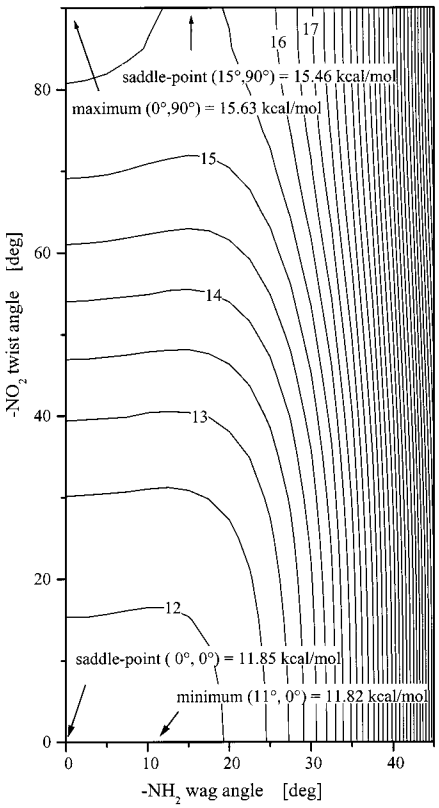

Figure 4. Heat of formation ΔH_0 (kcal/mol) of ground-state pNA in vacuo (calculated without configuration interaction). Here the dependence on $-NH_2$ wag and $-NO_2$ twist angles is shown.

When configuration interaction is included, a new minimum appears if $-NO_2$ is twisted by 90° against the benzene plane. Its heat of formation, relative to that of the planar structure above, is calculated variously in a band 0 $\pm$0.5 kcal/mol (cf. Figure 5c). The barrier between the two minima is obtained at 1−2 kcal/mol. Large number CI calculations tend to overestimate the contribution of electron correlation to the ground-state energy, and the new minimum is not corroborated experimentally.[45] This excess heat of formation is significant only at $-NO_2$ twist angles >60° where it is estimated as ~3 kcal/mol from comparison with calculations without CI. We assume that a similar overestimation of the CI contribution applies to the lower excited states, in which case the transition energies—the main aims of our investigation—are not affected.

However, the (unchanged) qualitative conclusion from Figure 4 is that there should be a broad distribution of $-NO_2$ twist angles at room temperature. We note here already that in the lowest electronically excited state, the driving force is directed toward increasing $-NO_2$ twist angles. This is why we concentrate mostly on this coordinate in the following sections.

Excited States and Optical Absorption Spectrum. For the ground-state equilibrium geometry, the vertical electronic transition energies and their oscillator strengths are collected in Table 4. The singlet transition which dominates the absorption spectrum is $S_4 \leftarrow S_0$ ($^1B_1$ ($\pi^* \leftarrow \pi$)) with oscillator strength f_{40} = 0.31. It is recognized in the experimental spectrum of pNA in the gas phase (Figure 1) as the strong band which peaks at 4.24 eV[15] (calculated: 4.56 eV). The weak and broad band which is observed around 3.5 eV represents transitions to the lower electronic states.

Figure 5 shows energies and properties as they depend on the internal rotation of $-NO_2$. In these SAM1 calculations all other geometrical parameters were allowed to relax. The

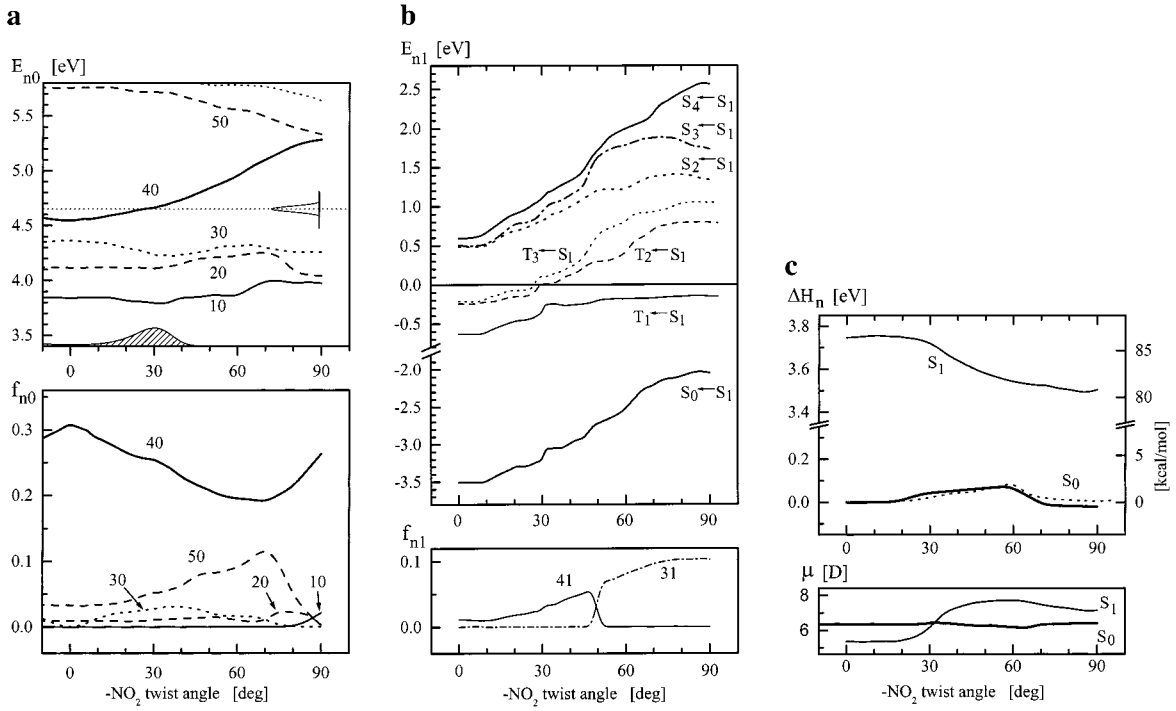

Figure 5. **(a)** Ground-state optical absorption of pNA in vacuo depending on $-NO_2$ internal rotation which is the main photochemical coordinate: vertical transition energies E_{n0} and oscillator strenghts f_{n0}, with all other parameters relaxed in S_0 (CI = 22). An example for spectral selection by a 40 fs excitation pulse is also indicated. **(b)** Excited-state absorption (n = 2,3..) or stimulated emission (n = 0) of pNA in vacuo depending on $-NO_2$ internal rotation: vertical $S_n \leftarrow S_1$ transition energies E_{n1} and oscillator strenghts f_{n1} (if larger than 0.02). Singlet−triplet $T_{1-3} \leftarrow S_1$ transition energies are also shown (CI = 16; all parameters except φ_{twist}^{nitro} relaxed in S_1). **(c)** Heat of formation ΔH_n and dipole moment μ for the ground and first excited state of pNA in vacuo depending on $-NO_2$ internal rotation, with all other parameters relaxed in S_n (CI = 22 for the ground state and CI = 14 for the excited state. For comparison, the dotted line represents ΔH_0 calculated with CI = 14). Values are given relative to ΔH_0 of the planar ground state conformation.

TABLE 4: Vertically Excited Singlet States of pNA in Vacuo at the SAM1, CI = 22 Level with Transition Energies E_{n0}, Oscillator Strengths f_{n0}, Franck−Condon Excited State Dipole Moments μ, and Weights of the Dominating One-Electron Transitions

state $S_n^{(0)}$	character	E_{n0} (eV)	f_{n0}	μ (D)	dominating one-electron transitions	$E_{n0,exp}$ (eV) (ref 15)
$S_1^{(0)}$ ($^1A_2$)[a]	$n\pi^*$	3.84	0.00	5.0	72% [HO-2, LU] + 18% [HO-2, LU+2]	
$S_2^{(0)}$ ($^1B_2$)	$\pi\pi^*$	4.11	0.01	7.2	60% [HO, LU+1] + 18% [HO-1, LU]	
$S_3^{(0)}$ ($^1A_1$)	$n\pi^*$	4.36	0.00	2.8	44% [HO-5, LU] + 24% [HO-4, LU]	
$S_4^{(0)}$ ($^1B_1$)	$\pi\pi^*$	4.56	0.31	14.1	82% [HO, LU] + 4% [HO-1, LU+1]	4.24
$S_5^{(0)}$	$\pi\pi^*$	5.76	0.03	9.7	52% [HO, LU+2] + 14% [HO, LU+3]	5.48
$S_6^{(0)}$	πn^*	5.87	0.02	11.2	62% [HO, LU+3] + 16% [HO, LU+2]	5.66

[a] Electronic symmetry assuming a fully planar structure.

calculations were carried out with CI = 14, 16, and 22; they gave qualitatively similar results. For transitions from the ground state (Figure 5a), relaxation took place in S_0 after which the vertically excited, nonrelaxed states $S_{1-6}^{(0)}$ were calculated. Transitions from the lowest excited state (Figure 5b), i.e., excited-state absorption and stimulated emission, were calculated after relaxation in S_1 (resulting in nonrelaxed states $S_0^{(1)}$, $S_2^{(1)}$, $S_3^{(1)}$, etc.). The heat of formation of S_0 and S_1 as function of the $-NO_2$ twist angle is also shown (Figure 5c). Remember that in the electronic ground state nearly all $-NO_2$ twist angles should be populated at room temperature. Because of the dependence of the vertical transition energy E_{40} on the twist and wag angles, the corresponding ground-state absorption band should be broadened to 0.7 eV (in addition to broadening due to other vibronic structure). This can be compared with the experimental spectrum of gas-phase pNA which has full width at half-maximum of 0.67 eV.[15]

Femtosecond Optical Excitation and Vibronic Relaxation. Consider femtosecond optical excitation on the red edge of the dominant absorption band which produces an electronic state $S_4^{(*)}$ with a nonequilibrium nuclear distribution (indicated by the asterix). The dipole moment of this nonrelaxed state at the ground-state geometry, $S_4^{(0)}$, is calculated at 14 D which agrees with the value of 13.76 D obtained by ab initio calculations[7] and with the experimental data (cf. Table 1). It follows from the previous section that spectral selection results in a distribu-

tion of $-NO_2$ twist angles with preference of more coplanar conformations. For example in Figure 5a we indicate on the ordinate a 40 fs Gaussian pulse tuned to 4.65 eV and obtain the distribution shown on the abscissa with the classical reflection principle. The nuclear distribution will relax within the electronic S_4 state along its displaced normal coordinates and by intramolecular vibrational redistribution (IVR). Simultaneously, internal conversion (IC) transfers population to nearby $S_3^{(*)}$ and further to $S_1^{(*)}$. The dipole moment of the latter is calculated at 6 D close to that of the ground state.

Let us consider the fate of the distribution of $-NO_2$ twist angles, as initially prepared in S_4, during internal conversion $S_4^{(*)} \leftarrow S_1^{(*)}$. For this we varied $\varphi_{\text{twist}}^{\text{nitro}}$ in the ground state and calculated the vertically excitated states $S_1^{(0)}$ through $S_4^{(0)}$. The vertical transition energies E_{10}, E_{20}, and E_{30} in Figure 5a are all flat around $\varphi_{\text{twist}}^{\text{nitro}} = 0$; the excited states S_1, S_2, and S_3 have an energy minimum for the coplanar conformation with curvature similar to S_0 corresponding to a 50 cm^{-1} torsional vibration. At that frequency it takes approximately 350 fs (one-fourth of a torsional period) for $-NO_2$ to librate from a coplanar conformation to the classical turning point. To summarize: there are no structural differences between the excited states regarding this twisting coordinate, its initial distribution in $S_4^{(*)}$ is localized around $\varphi_{\text{twist}}^{\text{nitro}} = 0$, and the characteristic time scale for internal rotation is 350 fs. Assuming the time scale for $S_4^{(*)} \rightarrow S_1^{(*)}$ internal conversion $\tau_{\text{IC}} \sim 1/\nu_7$ from the frequency of the lowest stretching mode, we estimate $\tau_{\text{IC}} \approx 100$ fs. From all of the above it may be concluded that the spectral selection of $-NO_2$ twist angles should essentially survive IC to $S_1^{(*)}$. There it will broaden and attain its thermal distribution at the elevated temperature $T \approx 840$ K which results from internal conversion of 1 eV of excess photon energy.

How can this second stage, i.e., geometry relaxation within the $S_1^{(*)}$ state, be observed? For an answer we first discuss the structural changes which result from full optimization in S_1 starting from the S_0 geometry. The benzene moiety shrinks somewhat along the long molecular axis and elongates along the short axis while the C−N bond lengths stay almost unchanged. Other changes concern the $-NH_2$ group. The amino twist angle remains zero for the S_1 equilibrium geometry but the twisting frequency increases to 410 cm^{-1} (from 360 cm^{-1} in S_0). The double minimum along the amino wagging coordinate disappears in S_1 and the wagging frequency is now 270 cm^{-1}. All of the features above relate to a stable S_1 structure closest to the ground-state geometry. However, a wider search reveals the global S_1 minimum which has the nitro group twisted by 90° (with the energy lower by ~0.1 eV as compared with the planar geometry, cf. Figure 5c). On the way to this perpendicular conformation, the transition energies E_{n1} for excited-state absorption $S_n^{(1)} \leftarrow S_1^{(1)}$ and oscillator strengths f_{n1} are shown in Figure 5b. With increasing twisting of $-NO_2$, f_{41} increases from 0 to 0.1. Therefore, this stage of relaxation may be evidenced by a rise in excited-state absorption around 1.8 eV on a 0.5 ps time scale. Because of the flatness of the full potential energy curve and high temperature, a wide distribution of nitro twist angles will be established in thermal equilibrium.

The final relaxation stage, after 0.5 ps, is internal conversion $S_1 \rightarrow S_0$ and intersystem crossing (ISC) $S_1 \rightarrow T_1$. Radiative transitions can be excluded because stimulated emission $S_1^{(1)} \rightarrow S_0^{(1)}$ has very low oscillator strength (<0.01) for all twist and wag angles. Here we touch briefly on the relative probability for ISC in the coplanar and perpendicular $-NO_2$ conformations. The transition energies to the three lowest triplet states are shown in Figure 5b. In the coplanar conformation, the S_1 state may be characterized as $n\pi^*$ and below there are three triplet states of which T_1 and T_2 are $\pi\pi^*$ and T_3 is $n\pi^*$ in character. Remember that ISC is suppressed by symmetry when the participating singlet and triplet states are composed of essentially the same orbitals.[46] From the small energy difference $E(S_1) - E(T_2) \leq 0.2$ eV it can be concluded that transition $S_1(n,\pi^*) \rightarrow T_2(\pi,\pi^*)$ is favored for $-NO_2$ twist angles <30°. In the perpendicular $-NO_2$ conformation, however, the S_1 state attains $\pi\pi^*$ character and below there is only T_1 (with $E(S_1) - E(T_1) \approx 0.2$ eV) which is built essentially with the same orbitals: hence ISC should be smaller here compared to the coplanar case for electronic reasons. In intermediate conformations with $-NO_2$ twist angle between 30° and 60° the S_1 and T_1 orbitals have mixed character and the matrix element of the spin−orbit coupling operator will not be limited by symmetry; thus ISC can compete with IC.

pNA in Water. To study the behavior of pNA in water we calculated the properties of the molecule using the conductor-like screening model (COSMO).[37] It should be noted that this solvation model applies best to strongly polar solvents. Configuration interaction, when included in the calculations, was carried with 16 molecular orbitals. Calculations with acetonitrile as solvent showed nearly identical results to those with water. Below we will discuss only water but note that the model ignores specific solvation. (The latter is responsible for the increased broadening of the absorption band in water when compared to the acetonitrile or dimethyl sulfoxide solutions;[22] cf. Figure 1.) As with the gas phase, special attention was paid to the dependence on $-NH_2$ and $-NO_2$ twist and wag angles.

Four types of calculations were performed for a state S_x in water at a chosen twist or wag angle. *First type for x = 0,1, 2, ...*: all other geometrical parameters were relaxed on the ground-state potential energy surface with solvation included. Then at this molecular geometry and with the solvent polarization adjusted to the ground-state charge distribution, the desired state was calculated. It is generally denoted $S_x^{(\text{nuc,solv})}$ extending the notation of the previous section; in the present case $S_x^{(0,0)}$ with nuc = 0, solv = 0. *Second type for x = 1*: following ground-state optimization as before, one cycle of the open-shell SCF calculation for S_1 was carried out in order to produce, based on ground-state MOs, the S_x energy including solvation. This excited state $S_1^{(0,1)}$ is "nonrelaxed" since its intramolecular coordinates were obtained in the ground state but, as such, the solvent is in equilibrium with the excited-state charge distribution. *Third type for x = 1*: the geometry in the excited state was optimized resulting in the state $S_1^{(1,1)}$—full relaxation for the state S_1 requires solv = nuc = 1. Typically, one of the internal coordinate (for example the $-NO_2$ rotation angle) was fixed while all other coordinates were optimized. Thus, electronic potential energy curves, etc. were calculated. *Fourth type for x = 1*: as before but with an additional coordinate kept at some fixed value (for example the $-NO_2$ wag angle constrained to zero) resulting in a *partially* relaxed state $S_1^{(p,1)}$ for each setting of the coordinate variable.

Ground-State Geometry, Vibrational Modes, and Potential Energy Surface. The potential energy surface for ground-state pNA in water ($S_0^{(0,0)}$ calculated without CI) is shown in Figure 6. Only the dependence on the low-frequency internal coordinates of the amino (upper panel) and nitro group (lower panel) is of interest here. Now the surface is even shallower along $-NO_2$ rotation than in the gas phase. At the global minimum $-NO_2$ is coplanar with the benzene moiety and $-NH_2$ is wagged ($\varphi_{\text{wag}}^{\text{amino}} \approx 20°$) but not twisted.

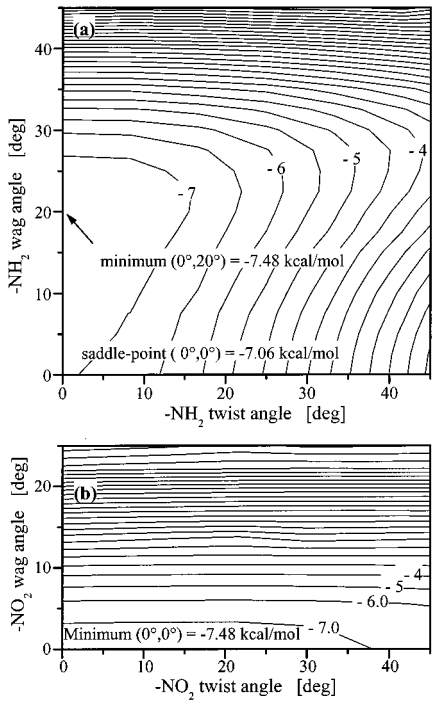

Figure 6. Heat of formation ΔH_0 (kcal/mol) of ground-state pNA in water (calculated without CI). Here the dependence on $-NH_2$ wag and twist (upper panel) and on $-NO_2$ wag and twist angles (lower panel) is shown.

The vibrational spectrum of $S_0^{(0,0)}$ at the global minimum was calculated with CI = 0 and 16. The $-NO_2$ twisting mode is predicted near 30 cm^{-1} and the $-NH_2$ wagging mode at 510 cm^{-1}. Comparison with the calculated gas phase frequencies shows that solvation strengthens $-NH_2$ wagging by more than 100 cm^{-1} while the other low-frequency modes stay almost unchanged. (The change of the $-NO_2$ twisting frequency is insignificant since it falls within the accuracy limits of the calculations. However, further below, this ground-state torsional frequency is determined to be 30 cm^{-1} from oscillations in the transient spectra.) The a_1 vibrational modes at 381 (340) cm^{-1} and 1412 (1261) cm^{-1} (scaled values[47] in brackets) involve benzene stretching and benzene-nitro (C4−N2, cf. Figure 3a) stretching motion, respectively. The calculated frequencies agree well with Raman frequencies of 390 and 1280 cm^{-1} observed in our transient spectra at zero time delay.[25] The latter mode (1460 cm^{-1} from ab initio RHF/6-31G(d) calculations in vacuo) is characterized by a symmetrical vibration of the $-NO_2$ group. It is responsible for a very strong line near 1310−1340 cm^{-1} in the Raman spectra of pNA in solutions[14,17,40] and was shown to give the largest contribution to all (hyper)polarizabilities of pNA.[8] Vibrational structure spaced by 1330 and 400 cm^{-1} was also recognized in the phosphorescence spectra of *N,N*-dimethyl-pNA in an organic glass at 77 K.[12]

Excited States and Optical Absorption Spectrum. The pertinent energies and properties are compiled in Figure 7 where their dependence on $-NO_2$ twisting is shown, and in Figure 8 which gives the dependence on $-NH_2$ wagging. They were calculated with CI = 16.

First we discuss the ground-state absorption spectrum. It was already mentioned that the heat of $S_0^{(0,0)}$ formation is practically independent of $-NO_2$ rotation (Figure 7c). The minimum along the $-NH_2$ wag angle (now at $\varphi_{wag}^{amino} \approx 25°$; Figure 8c) is more pronounced compared to the gas phase in agreement with the increase of the $-NH_2$ wagging frequency. From transition energies and oscillator strengths (Figures 7a, 8a) it is seen that the transition $S_1^{(0,0)} \leftarrow S_0^{(0,0)}$ is dipole allowed and dominates the absorption spectrum. The first excited state in water corresponds to the fourth excited state in the gas phase; solvation pulls this charge-transfer state below the other excited states because of its high dipole moment (see below). As $-NO_2$ is twisted away from $\varphi_{twist}^{nitro} = 0$, the oscillator strength f_{10} is reduced (Figure 7a). This may be partly offset by decreasing φ_{wag}^{amino} from its equilibrium value to zero. The maximum $f_{10} \approx 0.33$ of the completely planar structure (both substituents coplanar with the benzene moiety, with transition energy $E_{10} = 3.5$ eV) decreases with $-NO_2$ twisting to zero for the perpendicular conformation. As a consequence, again assuming a wide distribution of torsional angles in the electronic ground state, the HOMO−LUMO absorption band should be wide (∼0.6 eV; further broadening is provided by solvation) and asymmetric with its maximum near 3.5 eV at the low energy side. This is compared with the experimental absorption spectrum of pNA in water shown in Figure 1. The observed spectrum has an asymmetrical shape with a width of ∼0.7 eV and maximum at 3.25 eV. The oscillator strength $f_{10} = 0.31$ for at the equilibrium structure almost coincides with the experimental value of 0.32.[15]

The geometry of the charge-transfer state S_1 in water will be examined next. The fully planar structure of the ground state is now unstable. Instead, a deep minimum is attained by $-NO_2$ twisting to ∼80° which is the main photochemical reaction path (Figure 7c). When following this path we assume in our calculations that the water solvent is always equilibrated with the excited-state charge distribution (but see below). Yet for a given $-NO_2$ twist angle, for example, how should the remaining intramolecular degrees of freedom be chosen? In Figures 7 and 8 two representative cases are distinguished: the geometry is either adjusted in the ground state (internally "nonrelaxed" $S_1^{(0,1)}$) or it is optimized in the first excited state ("relaxed" $S_1^{(1,1)}$). Again it is instructive to characterize the change from the nonrelaxed to the relaxed structure for any given value of the $-NO_2$ twist coordinate. This intramolecular reorganization in S_1 consists mainly in a decrease of the $-NH_2$ wag angle from 25° to 0°, in a contraction of the amino-C bond by 0.05 Å, and in large changes of the C-nitro bond length depending on $-NO_2$ twist angle (Figure 7d). It accounts for 0.4−0.8 eV of the total intramolecular reorganization energy in S_1. At small $-NO_2$ twist angles the C−nitro bond is quite extended and the $S_1^{(1,1)}$ state can be considered as predissociating, thus offering another channel of energy relaxation.

Finally, for this section, intersystem crossing of pNA in water is discussed briefly. We find the lowest triplet above the fully relaxed singlet state by more than 0.1 eV for all φ_{twist}^{nitro} angles. Only in the partially relaxed excited state with $\varphi_{wag}^{nitro} = 0$, T_1 drops below $S_1^{(p,1)}$ at $\varphi_{twist}^{nitro} < 50°$ where both states have $\pi\pi^*$ character; their energy separation increases to 0.6 eV for angles below 20°. It follows that ISC should generally be impeded for electronic reasons, in agreement with experimental findings.[24] Comparing with the calculations in vacuo one expects resonant enhancement of ISC in weakly polar solvents for which the lowest excited singlet is still of $n\pi^*$ character and the T_1 and T_2 $\pi\pi^*$ states are shifted upward but are still below the S_1 state. This may explain the relatively high intersystem crossing rate of pNA in benzene.[21]

Femtosecond Optical Excitation and Vibronic Relaxation. Again we discuss ultrafast optical excitation at the red edge of the absorption band which produces an electronic state $S_1^{(*,*)}$ with nonequilibrium intramolecular and solvent distributions. Although all $-NO_2$ twist angles are populated in the ground

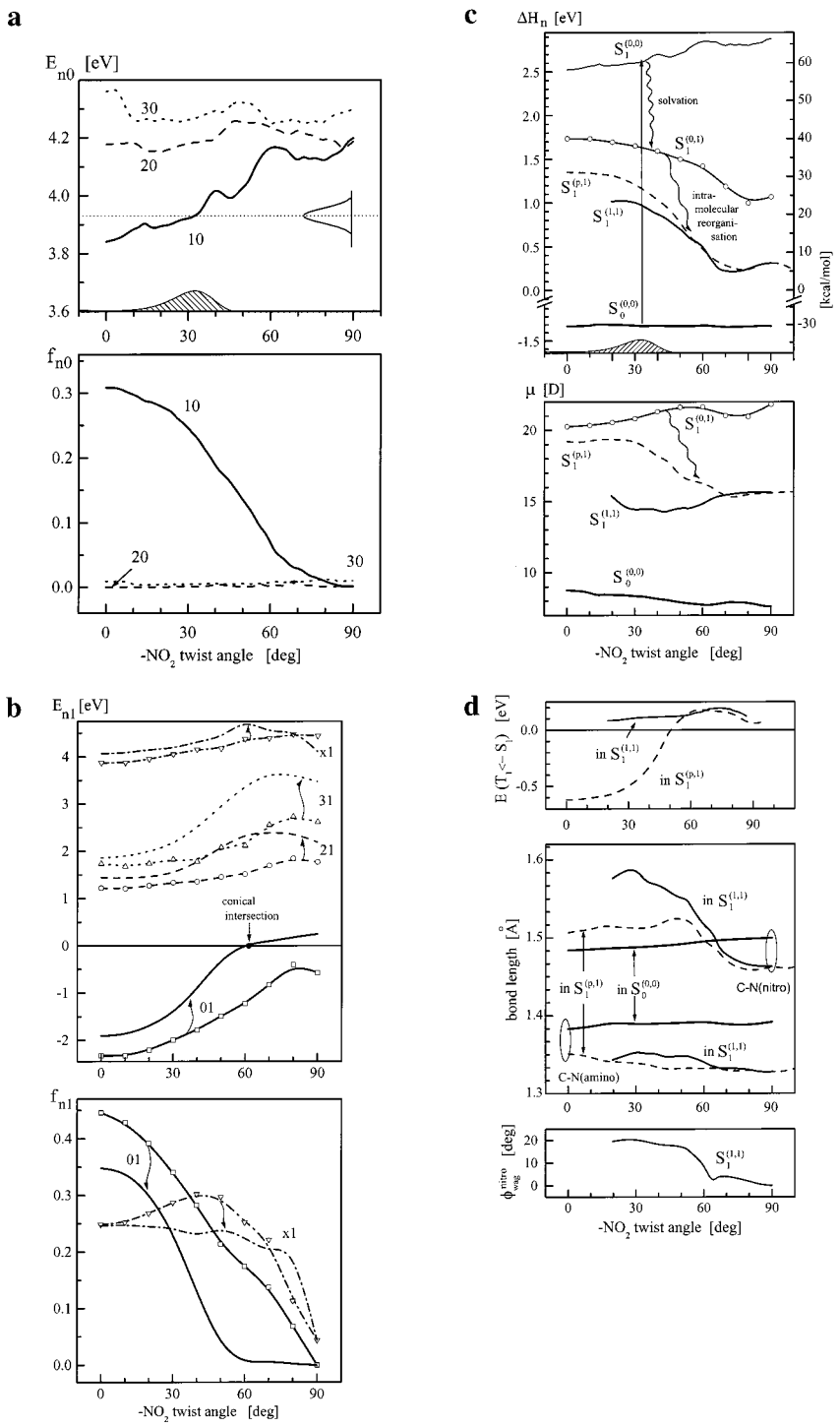

Figure 7. **(a)** Ground-state ($S_0^{(0,0)}$) absorption of pNA in water (CI = 16) depending on $-NO_2$ internal rotation: vertical transition energies E_{n0} and oscillator strengths f_{n0}. An example for spectral selection by a 40 fs excitation pulse is also indicated. **(b)** Excited-state absorption ($n = 2, 3, ...$) or stimulated emission ($n = 0$) of pNA in water (CI = 16) depending on $-NO_2$ internal rotation: vertical transition energies E_{n1} and oscillator strengths f_{n1}. Lines without symbols refer to transitions emanating from solvent-equilibrated $S_1^{(p,1)}$ which is partially relaxed ($\varphi_{wag}^{nitro} = 0$ and all remaining free intramolecular parameters relaxed). Lines with symbols indicate transitions from $S_1^{(0,1)}$ which is fully solvated but still has the ground-state geometry. Wavy arrows indicate change caused by intramolecular relaxation. Oscillator strengths for $S_{2,3} \leftarrow S_1$ transitions are below 0.02 and are not shown. **(c)** Heat of formation ΔH_n and dipole moment μ of pNA in water (CI = 16) depending on $-NO_2$ internal rotation for states $S_n^{(nuc,solv)}$ at different stages of relaxation. Optical excitation (the example in Figure 7a) creates a distribution of torsional angles in S_1. The Franck−Condon excited-state $S_1^{(0,0)}$ relaxes through ultrafast solvation to $S_1^{(0,1)}$ and by intramolecular reorganization to $S_1^{(1,1)}$, to be followed by nitro twisting. The dipole moment during the latter, slower process increases by only 2 D (lower panel). Other relaxation pathways may involve solvent-equilibrated $S_1^{(p,1)}$ which is partially relaxed ($\varphi_{wag}^{nitro} = 0$ and all remaining free intramolecular parameters relaxed). **(d)** Singlet−triplet $T_1 \leftarrow S_1$ splitting, C−N bond lengths and nitro wag angle for states $S_n^{(nuc,solv)}$ of pNA in water (CI = 16) depending on $-NO_2$ internal rotation at different stages of relaxation (see legend to Figure 7c).

state, their distribution in the excited state is weighted toward the coplanar conformation ($\varphi_{twist}^{nitro} \approx 0°$, $\varphi_{wag}^{amino} \approx 0°$) because of spectral and radiative selection. For example, Figure 7a shows the spectrum of a 40 fs pulse tuned to 3.9 eV. Optical excitation

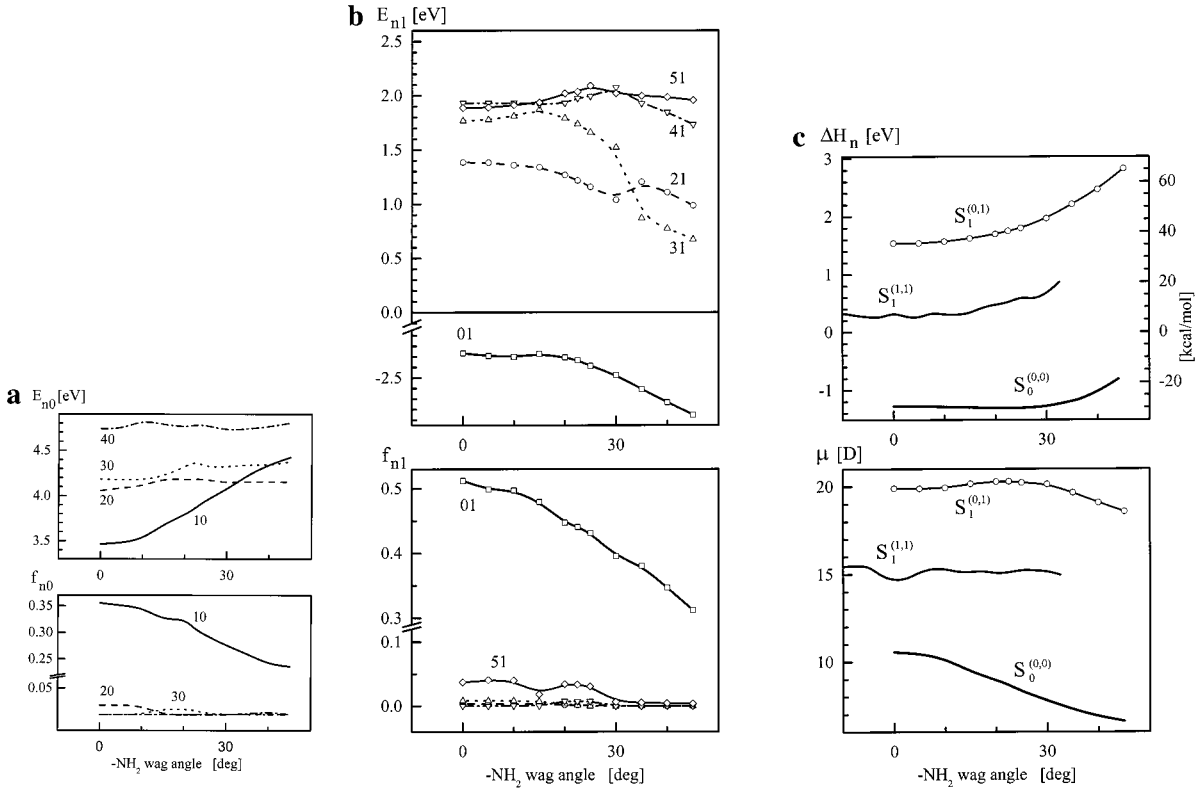

Figure 8. **(a)** Ground-state ($S_0^{(0,0)}$) absorption: vertical transition energies E_{n0} and oscillator strenghts f_{n0} of pNA in water (CI = 16) depending on $-NH_2$ wagging. **(b)** Transition energies E_{n1} and oscillator strengths f_{n1} for excited-state absorption (n = 2,3..) or stimulated emission (n = 0) of pNA in water (CI = 16) depending on $-NH_2$ wagging. The first excited-state $S_1^{(0,1)}$ is fully solvated but has the ground-state geometry. **(c)** Heat of formation ΔH_n and dipole moment μ for states $S_n^{(nuc,solv)}$ of pNA in water (CI = 16) depending on $-NH_2$ wagging, at different stages of relaxation (see legend to Figure 7c).

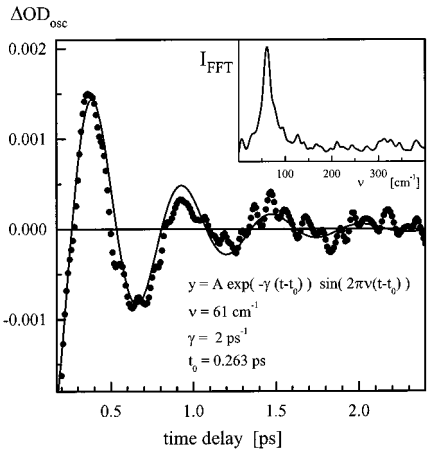

Figure 9. Oscillating part[48] ΔOD_{osc} of the kinetic trace[25] at E_{probe} = 2.51 eV with its fit by a damped sine function, in the time interval 0.18−5 ps. The Fourier power spectrum is shown as inset.

with this pulse produces a distribution around $\varphi_{twist}^{nitro} \approx \pm 30°$ as is indicated in the figure. A corresponding (symmetrical) hole is created in the ground-state distribution. Its oscillation in the ground state at frequency ω_{twist}^{nitro} around $\varphi_{twist}^{nitro} = 0°$ should produce a frequency modulation of the bleached ground-state absorption at 2 ω_{twist}^{nitro} because the $S_1^{(0,0)} - S_0^{(0,0)}$ energy gap has a symmetric minimum at the coplanar conformation. Indeed weak oscillations of the transient absorption signal are observed (Figure 9).[48] From their frequency of $\approx$ 60 cm^{-1}, a ground-state $-NO_2$ torsional frequency of 30 cm^{-1} must be concluded. In the excited electronic state, high-frequency stretching modes involving nitro−C and C−amino bonds should also be excited. They will modulate the dipole moment and therefore couple with the polar solvent through dipole−dipole interaction in addition to short-range coupling, for example due to H-bonds. The pertinent low-frequency modes couple dielectrically to the solvent through the (weak) dependence of the excited-state dipole moment on the twist and wag angles as was discussed above.

Immediately after impulsive excitation, the intramolecular driving force is directed toward larger nitro−C and smaller C−amino bond lengths, reduced amino wag angle, and toward the twisted nitro conformation. This force depends also on the polarization of the solvent and therefore solvation dynamics must be considered. The dipole solvation correlation function $C(t)$ of water has an ultrafast inertial component and an intermediate librational regime which together account for 60% of the relaxation by 100 fs.[49] The remainder of $C(t)$ is diffusive over a 1−10 ps time scale. The reorganization along the high-frequency C−N stretching coordinates is expected to occur on the same time scale or faster (due to intramolecular vibrational redistribution) than the ultrafast solvation components mentioned above. Thereafter, the remaining slower processes such as reorganization along the $-NH_2$ wagging and $-NO_2$ twisting coordinates are driven by their mean-field force, with the solvent polarization following adiabatically. Nitro twisting will now be discussed with the help of Figure 7 where the first excited state is treated at various stages of intramolecular equilibration. For example consider ground-state pNA with $\varphi_{twist}^{nitro} = 30°$ as selected by an appropriate excitation pulse (Figure 7a). For simplicity assume that all other parameters, in particular φ_{wag}^{amino}, are relaxed so that the process starts from $S_0^{(0,0)}$ (Figure 7c, upper panel). Excitation creates the Franck−Condon state $S_1^{(0,0)}$. If the latter is solvated ultrafast prior to any intramolecular rearrangement, then a state $S_1^{(0,1)}$ is reached. The dipole moment

increases from $\mu_0^{(0,0)} = 8.4$ D to $\mu_0^{(0,1)} = 20.8$ D during that process: evidence of the charge-transfer character of S_1 (Figure 7c, lower panel). The subsequent evolution of the dipole moment depends on the speed of $-NO_2$ twisting relative to relaxation of the other intramolecular coordinates. If the latter all relax much faster, the dipole moment thereby first drops to $\mu_1^{(1,1)} =$ 14.4 D after which nitro twisting causes a small increase to 15.6 D at the (final) perpendicular conformation. But other paths are also conceivable. For example, the nitro group may be kept not only from immediate twisting but also its wag angle may by constrained because of steric hindrance by the solvent (H-bonding). The corresponding excited state is $S_1^{(p,1)}$ which is fully solvated but partially relaxed since $\varphi_{wag}^{nitro} = 0°$. Its dipole moment before twisting is 19.2 D which is lowered to 15.6 D by subsequent nitro rotation. In summary we see that regardless of the actual path taken in S_1, nitro rotation to the perpendicular conformation is accompanied by a dipole moment change which has an upper limit of ca. 2 D. It follows that polar solvation of the twisted excited molecule does not contribute to the driving force and intramolecular charge transfer is not governed by this coordinate, and this is *not* twisted intramolecular *charge* transfer (TICT).

We now discuss the observations which are predicted by our calculations. They will be used to interpret the transient spectra recorded after excitation with 40 fs pulses (Figure 2). Therefore, the radiative transitions which emanate from S_1 are mainly examined here (Figures 7b, 8b). Remember that a range of angles for the nitro twist and amino wag coordinates is selected by optical pumping. Strong excited-state absorption $S_x \leftarrow S_1$ with oscillator strength $f_{x1} \approx 0.25$ is expected and observed at a transition energy $E_{x1} \approx 4$ eV. [S_x refers to a high-lying singlet state. For the nonrelaxed geometry $x = 11$ and for the partially relaxed geometry $x = 12$.] Only very weak excited-state absorption is predicted below so that the observed $\Delta OD < 0$ in that range may safely be described by a band for stimulated emission only. After ultrafast solvation, stimulated emission should be observed initially around 2.4 eV with oscillator strength $f_{01} \approx 0.44$ or smaller depending on the $-NO_2$ conformational distribution selected (Figure 7b). Nuclear rearangement along C−N stretching modes will have two effects: the ESA band shifts sightly to the blue, but more significantly, the SE band shifts to the red by 0.5 eV and suffers a reduction in amplitude because of reduced radiative coupling to the ground state. These expectations are essentially borne out by the observations although the calculated reorganization energies appear to be overestimated. The SE band observed at 40 fs delay time is still partly superimposed with ground-state bleaching; its mean transition frequency is estimated at 2.7 eV. Until 100 fs the mean frequency evolves toward 2.3 eV. After this stage, initial intramolecular relaxation and the major part of solvation may be considered completed. The next stage should consist of the $-NO_2$ twisting process followed or accompanied by internal conversion to S_0 and possibly intersystem crossing to T_1. The loss of S_1 population may be monitored by observing the ESA band since its transition energy and oscillator strength depend only weakly on the $-NH_2$ wag and $-NO_2$ twist angles. On the other hand, the transition energy for stimulated emission $S_1 \rightarrow S_0$ depends strongly on $-NO_2$ twisting, decreasing from 1.9 eV calculated for the coplanar conformation to zero at 60°. (From here on a gradual reduction of the $-NO_2$ twist angle followed by geometry optimization does not remove the $S_1^{(1,1)}/S_0^{(1,1)}$ degeneracy: a multidimensional conical intersection has been reached.) Also the SE oscillator strength should fall off rapidly for $\varphi_{twist}^{nitro} > 20°$. Altogether, the SE band should red-shift and disappear faster due to its angular dependence than does the ESA band. This effect may be seen in the lower panel of Figure 2. The red shift has proceeded down to ≈2 eV by 0.3 ps at which time the SE band almost disappears (10% amplitude remains) while the ESA is only halved. Referring to f_{01} (φ_{twist}^{nitro}), its reduction by a factor 0.2 corresponds already to a twist angle of 45° while the observed reduction by 0.1 corresponds to $f \approx$ 0.035 which is close to the calculation error. Thus we may conclude safely that the distribution over $-NO_2$ twist angles has progressed to $\langle\varphi_{twist}^{nitro}\rangle > 45°$. The relaxed mean SE frequency at this point is calculated around 0.8 eV, clearly at lower energy than observed. This discrepancy may indicate problems in describing electron correlation of the nearby S_1 and S_0 states. Another explanation may be that intramolecular relaxation other than $-NO_2$ twisting is incomplete. However, we conclude that the essential feature observed, namely different disappearance rates of the ESA and SE bands on the 0.1−0.5 ps time scale, can be linked to the internal rotation of the nitro group. Further work is in progress regarding the internal conversion process itself and the subsequent cooling of the hot ground state.

Conclusion

p-Nitroaniline (pNA) was investigated in the gas phase and in water. Among several semiempirical methods, we find the SAM1 Hamiltonian to be most suitable by comparing results with experimental data. The strong near-UV or visible absorption band corresponds to a charge-transfer (CT) transition. When optically excited into this band, the molecule experiences quite different electronic and structural changes in unpolar and polar environments. However, the calculations reveal a common feature: the key role played by the nitro group in the spectroscopy and dynamics of pNA through its nitrobenzene twisting motion. This behavior may be contrasted with that of dimethylaminobenzonitrile (DMABN) where, instead, the dimethylamino group is crucial for photoinduced charge-transfer dynamics. The difference is a consequence of the stronger nitro acceptor in pNA and the stronger dimethylamino donor in DMABN. We arrive at the following conclusions:

For pNA in the gas phase: The charge-transfer excited state seen in strong near-UV absorption corresponds to the S_4 state. A weak energy dependence of the ground state on H_2N- wagging and $-NO_2$ twisting coordinates combined with strong dependence in the S_4 state results in wide absorption band. Femtosecond excitation at its red edge selects $-NO_2$ twist angles around the coplanar conformation. This distribution is expected to survive internal conversion $S_4 \rightarrow S_1$ on a 100 fs time scale. In S_1 the potential energy surface is shallow along the $-NO_2$ twisting coordinate with a weak minimum now at the perpendicular conformation. The distribution broadens substantially, due to heating to ∼840 K caused by IC, and populates more perpendicular conformations on a 0.5 ps time scale. This may be observed by the rise of excited-state absorption (ESA) at 1.8 eV. There are no radiative transitions to the singlet ground state. Intersystem crossing should be favored for more coplanar conformations; it can be monitored through the decay of ESA.

For pNA in water: In the ground state, $-NO_2$ internal rotation is nearly free. Solvation stabilizes the charge-transfer excited state which now corresponds to S_1. Conformational broadening contributes significantly to the absorption width because of a strong dependence of the S_1 energy on the nitro twist angle. Femtosecond excitation at the red edge therefore selects $-NO_2$ twist angles around the coplanar conformation. Amino- and nitrobenzene stretching modes are also excited; their relaxation

is considered to be faster than the ultrafast component of solvation by water. After 100 fs the relaxation dynamics should consist mainly in an evolution along the $-NO_2$ twisting coordinate toward a deep (1 eV) minimum at the perpendicular conformation. Contrary to the DMABN case, the dipole moment change during that process has an upper limit of ca. 2 D; therefore, polar solvation does not contribute to the driving force. Fluorescence or stimulated emission should be observed for the first few hundred femtoseconds before reaching angles >45°. A conical intersection with the ground state is entered at 60°. The S_1 population decay can be monitored independent from the twisting process by observing excited-state absorption at 4 eV. All of these predictions are consistent with recent pump/supercontinuum probe measurements of pNA in water.[25]

The insertion of pNA into a rigid solvent matrix will hinder or restrict large-amplitude motion. At low temperature, hole-burning spectroscopy in polar (EPA, PMMA) and unpolar (Ar, Xe) environments should then allow the observation of vibronic structure and line shapes in a complementary approach to the electronic and structural dynamics of exited *p*-nitroaniline.

Acknowledgment. We thank Prof. James T. Hynes for helpful discussions and Heidi Steingraber for steady-state measurements. The Deutsche Forschungsgemeinschaft is gratefully acknowledged for financial support through the Leibniz program.

References and Notes

(1) Bigelow, R. W.; Freund, H.-J.; Dick, B. *Theor. Chim. Acta* **1983**, *63*, 177.
(2) Hiberty, P. C.; Ohanessian, G. *J. Am. Chem. Soc*. **1984**, *106*, 6963.
(3) Daniel, C.; Dupuis, M. *Chem. Phys. Lett.* **1990**, *171*, 209.
(4) Bredas, J. L.; Meyers, F. *Nonlinear Opt.* **1991**, *1*, 119.
(5) Karna, S. P.; Prasad, P. N.; Dupuis, M. *J. Chem. Phys.* **1991**, *94*, 1171.
(6) Sim, F.; Chin, S.; Dupuis, M.; Rice, J. E. *J. Phys. Chem.* **1993**, *97*, 1158.
(7) Mikkelsen, K. V.; Lio, Y.; Agren, H.; Jorgensen, P. *J. Chem. Phys.* **1994**, *100*, 8240.
(8) Champagne, B. *Chem. Phys. Lett*. **1996**, *261*, 57.
(9) Bella, S. D.; Lanza, G.; Fragala, I.; Yitzchaik, Sh.; Ratner, M. A.; Marks, T. J. *J. Am. Chem. Soc.* **1997**, *119*, 3003.
(10) Trueblood, K. N.; Goldish, E.; Donohue, J. *Acta Crystallogr*. **1961**, *14*, 1009.
(11) Czekalla, J.; Wick, G. *Z. Electrochem*. **1961**, *65*, 727.
(12) Khalil, O. S.; Seliskar, C. J.; McGlynn, S. P. *J. Chem. Phys.* **1973**, *58*, 1607.
(13) Liptay, W. In *Excited states*; Lim, E. C., Ed.; Academic Press: New York, 1974; Vol. 1, p 129.
(14) Harrand, M. *J. Raman Spectrosc.* **1974**, *2*, 15. Harrand, M. *J. Raman Spectrosc.* **1975**, *4*, 53.
(15) Millefiori, S.; Favini, G.; Millefiori, A.; Grasso, D. *Spectrochim. Acta* **1977**, *33A*, 21.
(16) Carsey, T. P.; Findley, G. L.; McGlynn, S. P. *J. Am. Chem. Soc*. **1979**, *101*, 4502.
(17) Schmid, E. D.; Moschalski, M.; Peticolas, W. L. *J. Phys. Chem.* **1986**, *90*, 2340.
(18) Sinha, H. K.; Yates, K. *Can. J. Chem*. **1991**, *69*, 550.
(19) Sinha, H. K.; Yates, K. *J. Am. Chem. Soc*. **1991**, *113*, 6062.
(20) Obi-Egdebi, N. O.; Iwebo, I. *Spectrochim. Acta A* **1992**, *48A*, 257.
(21) Schuddeboom, W.; Warman, J. M.; Biemans, H. A. M.; Meijer, E. W. *J. Phys. Chem.* **1996**, *100*, 12369.
(22) Mohanalingam, K.; Hamaguchi, H. *Chem. Lett.* **1997**, 157. Mohanalingam, K.; Hamaguchi, H. *Chem. Lett.* **1997**, 537.
(23) Woodford, J. N.; Pauley, M. A.; Wang, C. H. *J. Phys. Chem. A* **1997**, *101*, 1989.
(24) Tomsen, C. L.; Thøgersen, J.; Keiding, S. R. *J. Phys. Chem. A* **1998**, *102*, 1062.
(25) Kovalenko, S. A.; Schanz, R.; Farztdinov, V. M.; Hennig, H.; Ernsting, N. P. *Chem. Phys. Lett.* **2000**, *322*, 200.
(26) Kovalenko, S. A.; Dobryakov, A. L.; Ruthmann, J.; Ernsting, N. P. *Phys. Rev. A* **1999**, *59*, 2369.
(27) Grabowski, Z. R.; Dobkowski *Pure Appl. Chem.* **1983**, *55*, 245.
(28) Berden, G.; van Rooy, J.; Meerts, W. L.; Zachariasse, K. A. *Chem. Phys. Lett.* **1997**, *278*, 373.
(29) Chudoba, C.; Kummrow, A.; Dreyer, J.; Stenger, J.; Nibbering, E. T. J.; Elsaesser, T.; Zachariasse, K. A. *Chem. Phys. Lett.* **1999**, *309*, 357.
(30) Pérez Salgado, F.; Herbich, J.; Kunst, A. G. M.; Rettschnick, R. P. H. *J. Phys. Chem. A* **1999**, *103*, 3184.
(31) Parusel, A. B. J.; Köhler, G.; Grimme, S. *J. Phys. Chem. A* **1998**, *102*, 6297.
(32) Sudholt, W.; Sobolewski, A. L.; Domcke, W. *Chem. Phys.* **1999**, *240*, 9.
(33) Takezaki, M.; Hirota, N.; Terazima, M.; Sato, H.; Nakajima, T.; Kato, S. *J. Phys. Chem. A* **1997**, *101*, 5190.
(34) Levine, I. N. *Quantum Chemistry*; Prentice Hall: London, 1991.
(35) Dewar, M. J. S.; Jie, C.; Yu, J. *Tetrahedron* **1993**, *49*, 5003. Holder, A.; Dennington, R. D.; Jie, C. *Tetrahedron* **1994**, *50*, 627.
(36) AMPAC 6.02. 1998, Semichem, Inc. 7128 Summit, Shawnee, KS 66216. AMPAC 6.55. 1999, Semichem, Inc. PO Box 1649 Shawnee, KS 66222.
(37) Klammt, A.; Shüürman, G. *J. Chem. Soc., Perkin Trans.* **1993**, *2*, 779. Klammt, A. *J. Phys. Chem*. **1995**, *99*, 2224. Klammt, A. *J. Phys. Chem*. **1996**, *100*, 3349.
(38) Frisch, M. J.; Trucks, G. W.; Schlegel, H. B.; Scuseria, G. E.; Robb, M. A.; Cheeseman, J. R.; Zakrzewski, V. G.; Montgomery, J. A., Jr.; Stratmann, R. E.; Burant, J. C.; Dapprich, S.; Millam, J. M.; Daniels, A. D.; Kudin, K. N.; Strain, M. C.; Farkas, O.; Tomasi, J.; Barone, V.; Cossi, M.; Cammi, R.; Mennucci, B.; Pomelli, C.; Adamo, C.; Clifford, S.; Ochterski, J.; Petersson, G. A.; Ayala, P. Y.; Cui, Q.; Morokuma, K.; Malick, D. K.; Rabuck, A. D.; Raghavachari, K.; Foresman, J. B.; Cioslowski, J.; Ortiz, J. V.; Stefanov, B. B.; Liu, G.; Liashenko, A.; Piskorz, P.; Komaromi, I.; Gomperts, R.; Martin, R. L.; Fox, D. J.; Keith, T.; Al-Laham, M. A.; Peng, C. Y.; Nanayakkara, A.; Gonzalez, C.; Challacombe, M.; Gill, P. M. W.; Johnson, B.; Chen, W.; Wong, M. W.; Andres, J. L.; Gonzalez, C.; Head-Gordon, M.; Replogle, E. S.; Pople, J. A. *Gaussian 98*, revision A.3; Gaussian, Inc.: Pittsburgh, PA, 1998.
(39) The dipole moments from different references up to 1981 are cited in: McClellan, A. L. *Tables of Experimental Dipole Moments*; Rahara: El Cerrito, CA, 1974 and 1989. Vol. 2 and 3.
(40) Varsanyi, G. *Vibrational Spectra of Benzene Derivatives*; Academic Press: New York, 1969.
(41) Ram, S.; Yadav, J. S.; Rai, D. K. *Indian J. Phys.* **1985**, *59B*, 19.
(42) Within the accuracy of nitrogen atoms lying in the plane of phenyl ring, this definition coincides with that of ref 32. In the literature the pyramidalization angle or inversion angle is often used. The exact relation between the pyramidalization angle and wagg angle is $\theta_{pyr} = \text{arctg}\{[\text{tg}(\pi - \varphi_1)]\sin\varphi_{wag}\}$, where φ_1 is the C−N−O or C−N−H bond angle. For small $\varphi_{wag} < \pi/6$ and $\varphi_1 \leq 2\pi/3$ we have $\theta_{pyr} \approx 2\varphi_{wag}$.
(43) Holder, A. J.; Dennington, R. D. *J. Mol. Struct. (THEOCHEM)* **1997**, *401*, 207.
(44) Schneider, S.; Freunscht, P.; Brehm, G. *J. Raman Spectrosc*. **1997**, *28*, 305.
(45) Trotter, J. *Acta Crystallogr*. **1959**, *12*, 884; *Tetrahedron* **1960**, *8*, 13.
(46) Turro, N. J. *Modern molecular Photochemistry*; University Science Books: Sausalito, CA, 1991; Chapter 6.
(47) Hehre, W. J.; Radom, L.; Schleyer, P. v. R.; Pople, J. A. *Ab initio molecular orbital theory*; Wiley: New York, 1986.
(48) The experimental conditions are described in ref 25. The oscillating part of a kinetic trace is given by the residuals to a triexponential fit.
(49) Jimenez, R.; Fleming, G. R.; Kumar, P. V.; Maroncelli, M. *Nature* **1994**, *369*, 471.